VPS VIBRATIONS IN PHYSICAL SYSTEMS

DOI: 10.21008/j.0860-6897.2022.3.01
Vibrations in Physical Systems, 2022, 33(3), 2022301

Impact of Cavity Edges Shape on Aerodynamic Noise

Paweł ŁOJEK, Ireneusz CZAJKA

AGH University of Science and Technology, Department of Power Systems and Environmental Protection Facilities, 30 Mickiewicza Av., 30-059 Kraków, Poland

Corresponding author: Paweł ŁOJEK, email: lojek@agh.edu.pl

Abstract In this article, the analysis of influence of cavity edge shapes on flow-generated noise is performed. The acoustic wave propagation in the channel, that result from the flow, was analyzed. Shape of upstream and downstream edges was modified. The hybrid method based on Navier-Stokes and Perturbed Convective Wave Equation was used to solve the unidirectional coupling. The research showed a significant influence of the modification of the shape of the cavity edges on the generated noise. The change of downstream corner allowed for significant reduction of noise in the entire analysed band and allowed for the reduction of overall sound pressure level (OASPL) by 5 dB. Modifications of the upstream edge did not bring such differences, change in OASPL was up to 1 dB. The obtained spectra of the sound pressure level showed compliance with the calculated natural frequencies of the analysed object, as well as with some of the Rossiter modal frequencies, typical for the phenomena occurring in the cavities.

Keywords: Aeroacoustics, fluid-acoustic coupling, cavity noise.

1. Introduction

The flow over the cavity is used to model the phenomena occurring in real objects with cavity-type geometry. As stated by Rockwell and Naudascher [1], cavity flows can be used as a model of phenomena occurring in, for example, slotted-wall wind and water tunnels, high-head gates, and aircraft components. There are many flow and acoustic phenomena associated with complex feedback and self-sustaining oscillations occurring in the cavities. This feedback loop consists of the following [2]: generation of pressure fluctuations in the impingement region which propagate upstream of the flow, shedding and amplification of instabilities at upstream edge of cavity, impingement of the vortices and instabilities at downstream wall/edge of the cavity, generation of new pressure fluctuations that propagate upstream, closing the loop. These oscillatory phenomena, especially the impingement, can cause the formation of an acoustic wave which then propagates into the space above the cavity.

This is an unwanted behaviour and since the beginning of research on the cavities, attempts have been made to control and reduce the oscillations and the generated noise. Both active and passive control strategies are used to change the behaviour of the flow. The active methods include the use of piezoelectric actuators placed before the upstream edge [3], vibrating plate located at downstream edge of the cavity [4] or pair of loudspeakers [5]. Passive methods usually consist in modifying the geometry of the cavity [6,7,8] or adding additional elements – array of Helmholtz resonators located near the downstream edge [9] or cylindrical rod in the crossflow [10].

In this research, an attempt was made to passively control the noise generated by the flow over the cavity. It was analysed, how the acoustic field generated by the flow changes, depending on the shape of upstream and downstream cavity edge. This work is a continuation of the research described in [6]. In former work, the analysis was based on acoustic analogies of Lighthill [11] and Curle [12], while in this study, a more precise (but also much more computationally expensive) approach [13], based on hybrid method, using Navier-Stokes equations to solve flow field and Perturbed Convective Wave Equation (PCWE) to compute flow-acoustic coupling and acoustic propagation.

2. Methods and algorithms

To solve the flow-induced noise problem, the hybrid method is incorporated. The method itself is based on the assumption of Hardin and Pope [14], developed further by Kaltenbacher [15]. It states that physical quantities that describe the flow can be split into mean ($\overline{p}, \overline{\mathbf{v}}, \overline{\rho}$), incompressible ($p^{ic}, \mathbf{v}^{ic}, \rho^{ic}$) and acoustic ($p^{a}, \mathbf{v}^{a}, \rho^{a}$) parts ($p$—pressure, $\mathbf{v}$—velocity, ρ—density) [16]. It allows to transform the compressible

Navier-Stokes equations into a system of acoustic perturbation equations (APE) [17], that can be further simplified to classical wave equation with source terms – substantial derivative of the incompressible pressure of the flow. This formula is called perturbed convective wave equation (PCWE) and is given by [17]:

$$\frac{1}{c^2}\frac{\mathrm{D}^2\psi^a}{\mathrm{D}t^2} - \Delta\psi^a = -\frac{1}{\overline{\rho}c^2}\frac{\mathrm{D}p^{ic}}{\mathrm{D}t}, \tag{1}$$

where $\frac{\mathrm{D}}{\mathrm{D}t} = \frac{\partial}{\partial t} + \mathbf{v}\cdot\nabla$ is the substantial (material) derivative, ψ^a is the acoustic velocity potential, ($p^a = \overline{\rho}\frac{\mathrm{D}\psi^a}{\mathrm{D}t}$ is the acoustic pressure, $\mathbf{v}^a = -\nabla\psi^a$ is the particle velocity). This equation allows for computations of acoustic wave propagation with flow sound sources.

The hybrid method consists of three parts: a) performing the flow simulations in the flow domain, on flow mesh; b) computing the source terms (time derivative of p^{ic}, flow pressure) and interpolation from flow to acoustic mesh and c) solving the PCWE (1) on acoustic mesh.

The necessity to use two different computational grids results from solving differential equations whose discretization differs from each other. CFD grids are often heterogeneous, they must be refined near the walls to properly resolve the boundary layer, while acoustic grid element size should be of the same size, to avoid reflections and numerical errors resulting from size change.

2.1. Incompressible flow

The first part of the hybrid aeroacoustic algorithm is to perform the simulations of unsteady incompressible flow. It is done by solving Navier-Stokes equations given by continuity (2) and momentum (3) conservation equations [13]:

$$\nabla\cdot\mathbf{v}^{ic} = 0, \tag{2}$$

$$\rho^{ic}\frac{\partial\mathbf{v}^{ic}}{\partial t} = +\rho^{ic}\mathbf{v}^{ic}\cdot\nabla\mathbf{v}^{ic} = -\nabla p^{ic} + \nabla\cdot\boldsymbol{\tau} + f_{\Omega}, \tag{3}$$

where $\boldsymbol{\tau}$ is the viscous stress tensor, f_{Ω} is the external forces per unit volume.

They were solved with finite-volume method implemented in OpenFOAM software [19]. We used $k-\omega$ SST Detached Eddy Simulation (DES) method, developed by Strelets [20], to model the flow. This method combines the Large Eddy Simulation (LES) and Reynolds-Averaged Navier-Stokes (RANS) methods. It allows for switching between these models and solving RANS equations in the boundary layer and LES equations outside it based on the grid size and flow parameters [16]. This method also enables obtaining accurate results while maintaining a reasonable computational time.

The second-order upwind schemes were used to compute convective terms, while for diffusive terms, methods incorporating Gauss theorem with scalar limiter were used. The equations describing the flow were solved with pressure implicit with splitting of operators (PISO) algorithm of Issa [21], resulting systems of algebraic equations were solved with geometric agglomerated algebraic multigrid (GAMG) solver.

2.2. Source terms interpolation

Procedure of source terms interpolation from CFD to acoustic mesh consist of the following steps and is described in greater detail in [18]. As a result of CFD calculations, the nodal values of pressure are known. First step is to conduct nearest neighbor interpolation of pressure values between nodes of CFD and acoustic mesh. The second – is to convert the nodal values of pressure to values in element centroids. Then, the cut-volume cell-based interpolation is performed. This cut-volume method conservates energy both globally and in each acoustic element and allows to avoid numerical errors. It should also be mentioned that this method is based on interpolation of the entire right side of the Finite-Element formulation of the PCWE equation (1).

2.3 Acoustic wave propagation

As mentioned before, the propagation of the acoustic wave is governed by perturbed convective wave equation (1). To be solved by a finite element method, it must be rewritten in variational form:

$$\frac{1}{c^2}\left(\int_\Omega \phi \frac{\partial^2 \psi^a}{\partial t^2}\mathrm{d}\xi + 2\int_\Omega \phi\,(\overline{\mathbf{v}}\cdot\nabla)\frac{\partial \psi^a}{\partial t}\mathrm{d}\xi + \int_\Omega (\overline{\mathbf{v}}\cdot\nabla)\,\phi(\overline{\mathbf{v}}\cdot\nabla)\psi^a \mathrm{d}\xi\right) + \int_\Omega \nabla\phi\nabla\psi^a \mathrm{d}\xi - \int_\Gamma \phi \frac{\partial \psi^a}{\partial n}\mathrm{d}S$$
$$= -\frac{1}{\overline{\rho}c^2}\int_\Omega \phi\left(\frac{\partial p^{ic}}{\partial t} + \overline{\mathbf{v}}\cdot\nabla p^{ic}\right)\mathrm{d}\xi, \qquad (4)$$

where ϕ is the test function.

The equation then discretized and solved with finite-element method with Lagrangian finite elements implemented in OpenCFS software, described in greater detail in [13]. The second-order finite difference scheme is used for time discretization. The resulting algebraic system of equations is solved with PARDISO solver.

3. Simulation set-up

The geometry of the case is shown in the Figures 1 and 2. The former shows the model used for the flow computations, while the latter – for the wave propagation case. In the Figures 1 and 2, the reference model, with perpendicular edges is shown. In all cases, the flow over cavity with a length to depth ratio of 2 was analysed.

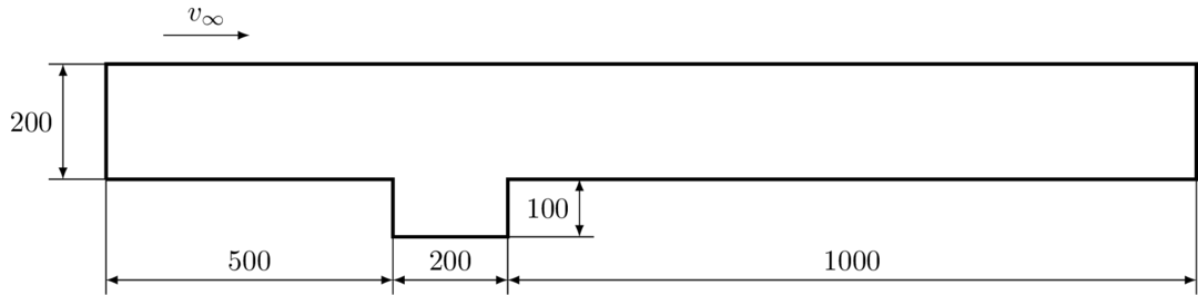

Figure 1. Geometry of the flow domain.

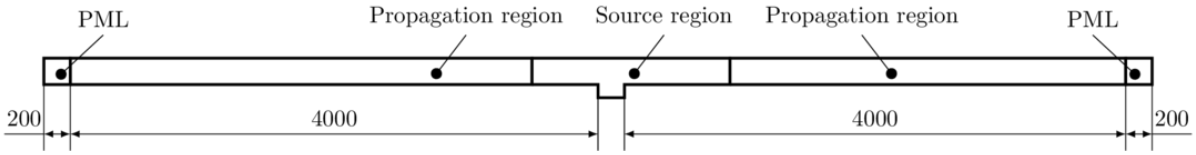

Figure 2. Geometry of the acoustic domain with marked regions.

In addition to the reference case (hereinafter RC) simulations were performed for different corner configurations. They are presented in the Fig. 3. For chamfered cases (a), b)), the edges were cut at angle of 45° on ¼ of the depth of the cavity, while for the rounded ones (c), d)), the radius was also equal to ¼ of the depth.

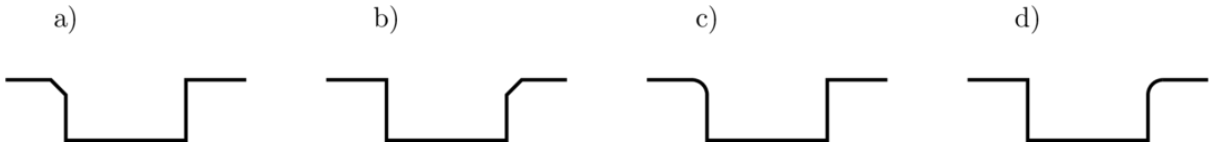

Figure 3. Analysed configuration of edges, a) chamfered upstream (CU), b) chamfered downstream (CD), c) rounded upstream (RU), d) rounded downstream (RD).

The computational mesh for finite-volume simulations of the flow was generated with cfMesh software, and for finite-element acoustic computations, with GMSH mesher. The dimensions of the volumes and elements were determined on the basis of mesh convergence study. In the case of CFD mesh, the size of the elements was also dictated by the need to resolve the boundary layer, the mesh had to be refined in near-wall region. Base element size was equal to $2 \cdot 10^{-3}$ [m], and wall adjacent cell height was equal to $1 \cdot 10^{-4}$[m]. The size of element for acoustic simulations in all cases were equal to $5 \cdot 10^{-3}$ [m]. Following the

principle of at least 6 elements per wavelength, this allowed for analyses of wave propagation with frequencies up to 11kHz.

3.1 Initial and boundary conditions

The flow over the cavity at a speed of 15 m/s was analysed. Values of turbulence kinetic energy k and speciffic dissipation ratio ω, required by the selected turbulence model ($k-\omega$ SST DES) were determined on the basis of the recommendations described in [22]. Air with a temperature of 20 °C was assumed as the analyzed fluid, with density $\rho = 1.204\ \mathrm{kg}/m^3$. Initial values were determined with the steady-state RANS solution obtained with SIMPLE algorithm of Spalding and Patankar [23].

The acoustic domain was divided into three parts (Fig. 2). In the source region, the source term interpolation was performed, the mesh of this region and CFD mesh overlaps. Due to possible numerical errors resulting from jump between source and propagation region, spatial blending function has to be introduced. RHS of the equation (4) is to be multiplied with blending function $f(x)$ given by:

$$f(x) = \begin{cases} \exp\left(\dfrac{-0.1((x-0.1)^2+y^2)}{\sigma^2}\right) & \text{if } \sqrt{(x-0.1)^2+y^2} < 0.2 \\ 0 & \text{otherwise.} \end{cases} \tag{5}$$

It should be noted that function (5) and parameter $\sigma = 0.05$ has some effect on computed acoustic pressure amplitudes. It has a certain influence on the acoustic pressure amplitudes, it is related to what percentage of the flow pressure is taken into account for the generation of the acoustic wave. It will be necessary to determine the value of the function on the basis of experimental research. The conducted analyzes showed, however, that it has no significant influence on the frequency composition of the computed acoustic pressure.

In the PML region, the perfectly matched layer (PML) technique described in [13] was used to model the free field radiation without any reflections. All cavity and channel walls were treated as acoustically hard. All regions were connected by conforming interfaces.

4. Results and discussion

To be able to assess the quality of the results obtained in the calculations, the eigenfrequencies of the system shown in the Fig. 2 were determined on the basis of the FEM simulation. Only the propagation and source regions were analyzed, the PML region was not analyzed. The channel walls were assumed to be rigid, while inlet and outlet were assumed to be open. In the simulations, the same results (up to 3 decimal places) were obtained for all edge shapes configurations. First fifteen eigenfrequencies had the following values: 20.7, 42.0, 62.1, 84.1, 103.4, 126.1, 144.8, 168.1, 186.2, 210.1, 227.6, 252.1, 269.0, 294.1, 310.3.

Acoustic and flow-related oscillation in the cavities can be described with Rossiter modes [24]. They can be determined based on the formula (6), describing the frequency of periodic fluctuations in cavity flows [24].

$$f_m = \frac{U}{L} \cdot \frac{m-\gamma}{\frac{1}{K}+M}, \tag{6}$$

where: U is the flow velocity, L is the length of the cavity, m is the mode number, $M = \left|\mathbf{v}^{ic}\right|/c$ is the Mach number, K is the ratio of vortex convection speed to the flow velocity, γ is the parameter describing the phase delay between hydrodynamic forces and the acoustic feedback [25]; for small Mach numbers γ is equal to 0.

Parameter K was computed based on the cross-correlation between velocity measured in two points in the flow and was equal to 0.65. First few Rossiter modes for analysed cavity flow had the following values: 47.4, 94.8, 142.2, 189.6, 237.0, 284.3, 331.7, 379.1.

Calculated eigenfrequencies and Rossiter modes will be compared with acoustic pressure spectrum. The structure of the flow field for the reference case at selected timestep is shown in the Fig. 4 by the distribution of velocity. The typical structure of the cavity flow can be seen, including the presence of two primary vortices in the cavity which form the recirculation zone, shear layer separation at upstream and its impingement at downstream edge, there is also a partial ejection of vortices from the cavity [2]. The occurrence of these phenomena proves that the flow simulations were carried out correctly. Similar flow behavior occurred in the remaining cases, with chamfered and rounded edges. However, as a result of the edge shape changes, the size and number of primary vortices in the cavity changed, which was previously shown in [6].

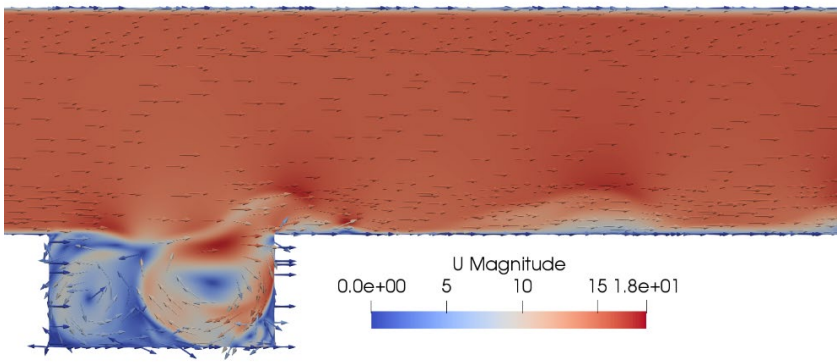

Figure 4. Velocity distribution of the flow over cavity at time t =1.2 s.

In the Figures 5-7, the power spectral densities of computed acoustic pressure are shown. The pressure was measured at probe located at the right end of the channel, before PML zone. In the Fig 5. the PSD for reference case is shown, while in the Fig. 6 and 7, the PSD for modified edges compared to the reference are shown. The computed spectra had the frequency resolution of 1 Hz. In all cases some of the natural frequencies as well as the Rossiter frequencies are excited. This is especially true in the reference case for the first nine eigenfrequencies and the first three Rossiter frequencies. In cases with altered geometry, there may have been some change in the frequencies excited by the flow, which are not accounted for by the Rossiter model.

In addition, there has been a decrease in PSD and hence the sound pressure level in cases with an altered downstream edge. Calculations showed a 3.5% (4 dB) decrease in overall sound pressure level for the downstream rounded edge, 4.4% (5.2 dB) for the downstream chamfered edge, 0.2% (0.3 dB) for the upstream rounded edge and 0.7% (0.6 dB) for the downstream chamfered edge compared to the reference case.

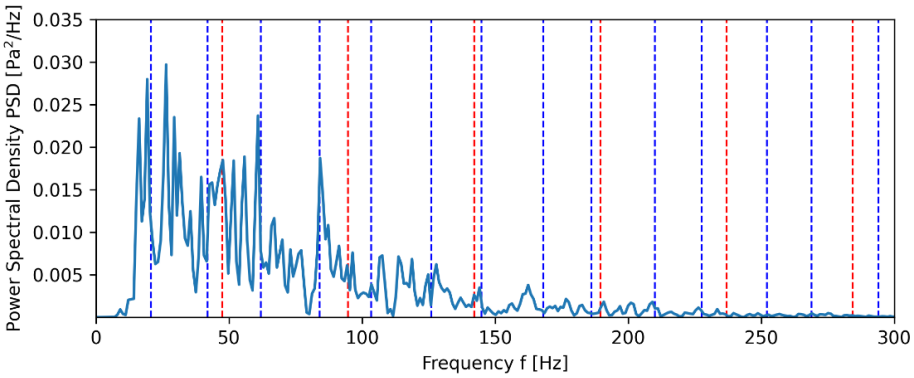

Figure 5. Power Spectral Density of pressure (—— -reference case, - - - - eigenfrequency, - - - - Rossiter mode).

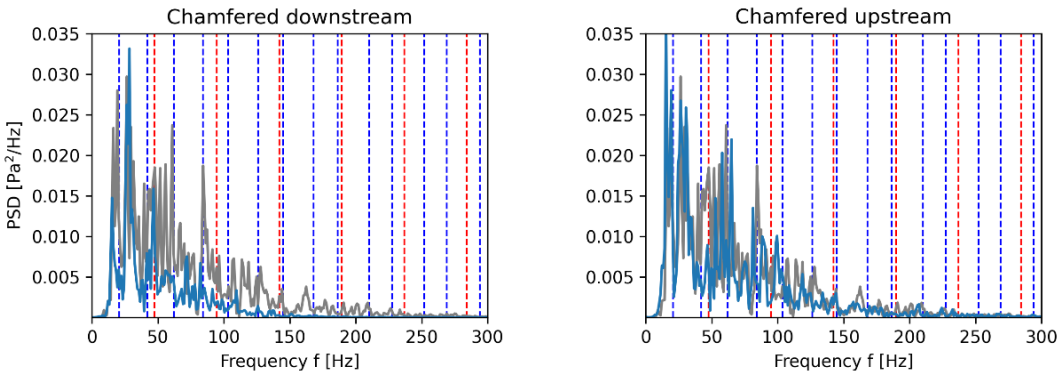

Figure 6. Power Spectral Density of pressure (—— -modified edge, —— -reference case, - - - - eigenfrequency, - - - - Rossiter mode).

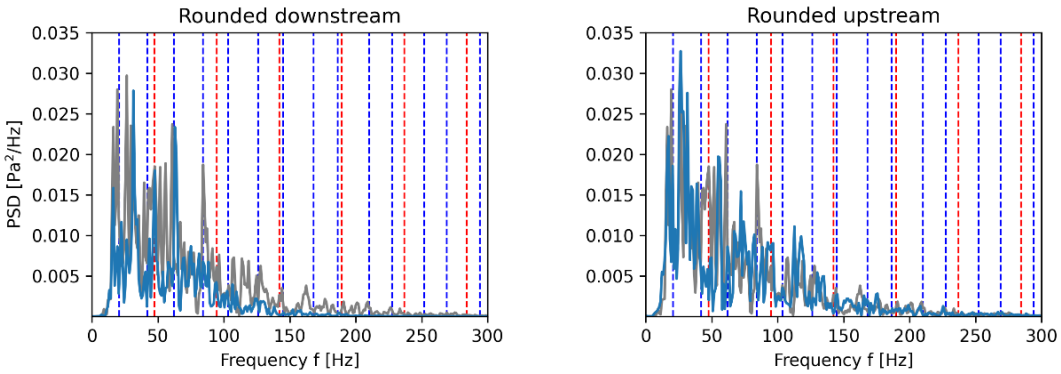

Figure 7. Power Spectral Density of pressure (—— - modified edge, —— - reference case, ---- eigenfrequency, ---- - Rossiter mode).

In the Figures 8, 9 and 10, the instantaneous acoustic intensity distribution in the cavity was shown. In each case that acoustic energy outflows from the cavity and is transported along the channel. The intensity distribution in the cavity largely depends on the flow pressure distribution and changes as the flow develops. By comparing the flow pressure and acoustic intensity distributions, it is possible to identify the zones that are responsible for the formation of an acoustic wave. Besides, the cavity edges are areas of increased intensity [26].

In addition, there is a difference in the acoustic intensity values between the reference and cases with modified downstream edge. The difference in maximum intensity is one order of magnitude.

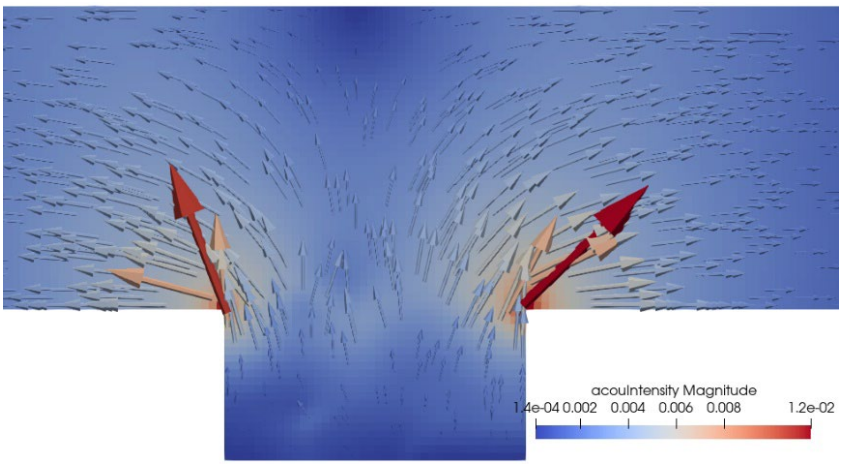

Figure 8. Instantaneous acoustic intensity distribution, reference case.

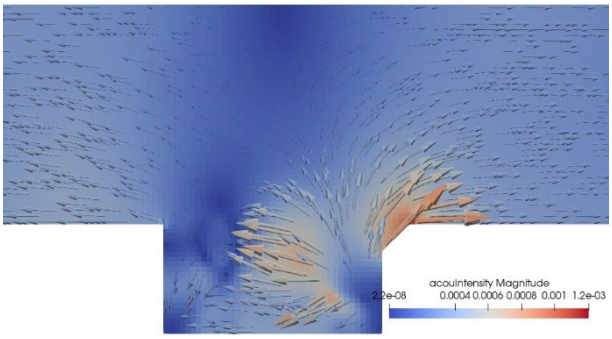

Figure 9a. Instantaneous acoustic intensity distribution, chamfered downstream edge.

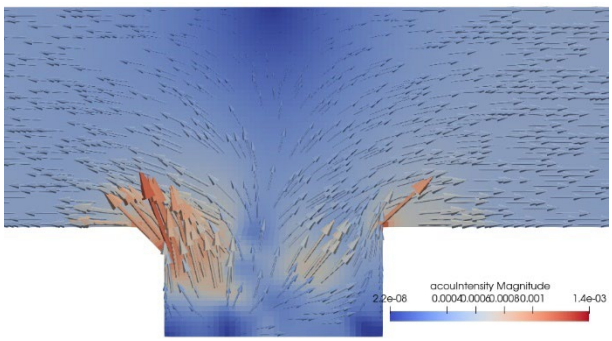

Figure 9b. Instantaneous acoustic intensity distribution, chamfered upstream edge.

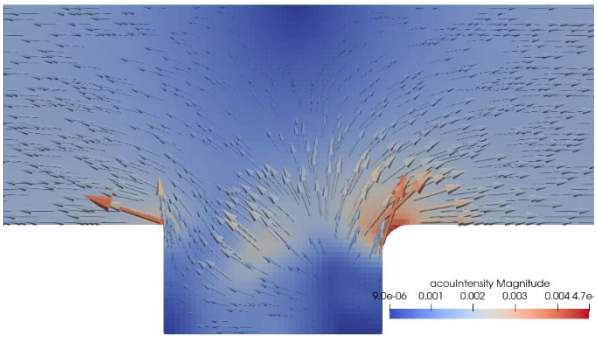

Figure 10a. Instantaneous acoustic intensity distribution, rounded downstream edge.

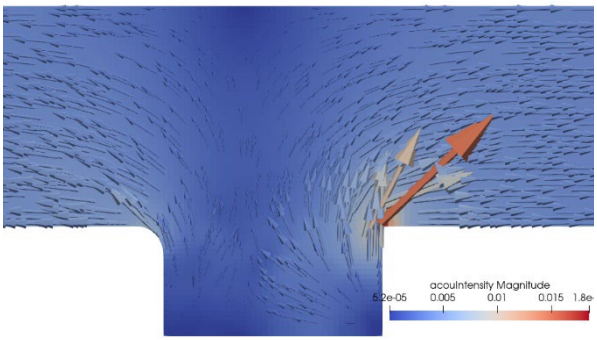

Figure 10b. Instantaneous acoustic intensity distribution, rounded upstream edge.

5. Conclusions

In the present study, the analysis of the flow-induced acoustic field over the cavity is performed. For this purpose, a hybrid method was used, which consists in calculating the source terms of the perturbed convective wave equation based on a flow simulation, and then solving this equation. The solution of Navier-Stokes and perturbed convective wave equations were obtained with finite-volume and finite-element codes – OpenFOAM and OpenCFS respectively.

The results confirm the assumptions presented in the introduction that the change of the cavity edges may be a method of passive reduction method of flow-generated noise. The modifications of the shape of the downstream edge of cavity resulted in a drop in variables describing the acoustic field – acoustic pressure and intensity. It was also shown that the upstream edge modifications did not have any significant positive effect on the sound pressure. The calculated spectra show that the edge change may cause an increase in power spectral density for some frequencies compared to the reference case.

The obtained conclusions are in line with those of the previous research [6], when the less complex model was used, i.e., acoustic analogies.

Although the wave propagation model used allows for considering convective effects, the presented calculations were made without taking them into account. Preliminary studies have shown that for such low flow velocities, convective effects are negligible.

Acknowledgments

This research was supported in part by PLGrid Infrastructure.

Additional information

The author(s) declare: no competing financial interests and that all material taken from other sources (including their own published works) is clearly cited and that appropriate permits are obtained.

References

1. D. Rockwell, E. Naudascher; Review – Self-Sustaining Oscillations of Flow Past Cavities; J. Fluids Eng. 1978, 100(2), 152-165. DOI: 10.1115/1.3448624
2. X. Gloerfelt, Cavity Noise, 2007.
3. S. Kikuchi, Y. Fukunishi, Active flow control technique using piezo-film actuators applied to the sound generation by a cavity, Proceedings of the 3rd ASME/JSME Joint Fluids Engineering Conference, 1999.
4. L. Chatellier, J. Laumonier, Y. Gervais, Active control of the aeroacoustics of cavity flows from the downstream edge, C. R. Mecanique 2006, 334(4), 259-265, DOI: 10.1016/j.crme.2006.03.003
5. D. R. Williams, D. Fabris, K. Iwanski, J. Morrow, Closed-loop control in cavities with unsteady bleed forcing, AIAA-2000-0470, 2000.
6. P. Łojek, K. Suder-Dębska, M. Mach, Influence of Cavity Edges Shape on Flow Induced Noise, Vibrations in Physical Systems 2021, 32(1), 2021110.
7. J.C.F. Pereira, J.M.M. Sousa, Influence of Impingement Edge Geometry on Cavity Flow Oscillations, AIAA Journal 1994, 32(8), 1737-1740, DOI: 10.2514/3.12168
8. A. Rona, X.X. Chen, Control of Cavity Flow Oscillation through Leading Edge Flow Modification, 36th AIAA Aerospace Sciences Meeting and Exhibit, 1998.

9. J. S. Hsu, K.K. Ahuja, Cavity noise control using Helmholtz resonators, AIAA 96-1675, 1996.
10. M. J. Stanek, J.A. Ross, J. Odedra, J. Peto, High Frequency Acoustic Suppression – The Mystery of the Rod-in-Crossflow Revealed 2003, AIAA 2003-0007.
11. M.J. Lighthill, M.H. Newman, On sound generated aerodynamically I. General theory, Proceedings of the Royal Society of London. Series A. Mathematical and Physical Sciences 1952, 211(1107).
12. N. Curle, The Influence of Solid Boundaries upon Aerodynamic Sound, Proceedings of the Royal Society 1955, 231, 505-514.
13. M. Kaltenbacher, Numerical Simulation of Mechatronic Sensors and Actuators. Finite Elements for Computational Multiphysics, Springer Science+Buissness Media, 2015.
14. J.C. Hardin, D.S. Pope, An Acoustic/Viscous Splitting Technique for Computational Aeroacoustics, Theoretical and Computational Fluid Dynamics 1994, 6, 5-6.
15. M. Kaltenbacher et al., Computational aeroacoustics for rotating systems with application to an axial fan, AIAA Journal 2017, 55(11). DOI: doi.org/10.2514/1.J055931
16. I. Czajka, Modelowanie zjawisk akustycznych w przepływach aerodynamicznych, Wydawnictwa AGH, 2019.
17. R. Ewert, W. Schroder, Acoustic Perturbation equations based on flow decomposition via source filtering, Journal of Computational Physics 2003, 188(2), 365-398.
18. S. Schoder et al, Application Limits of Conservative Source Interpolation Methods Using a Low Mach Number Hybrid Aeroacoustics Workflow, Journal of Theoretical and Computational Acoustics 2021, 29(1), 2050032. DOI: 10.1142/S2591728520500322
19. H.G. Weller, G. Tabor, H. Jasak, C. Fureby, A tensorial approach to computational continuum mechanics using object-oriented techniques, Computers in Physics 1998, 12(6), DOI: 10.1063/1.168744
20. M. Strelets, Detached Eddy Simulation of massively separated flows, 39th Aerospace Sciences Meeting and Exhibit, 2001.
21. R. Issa, Solution of the implicitly discretized fluid flow equation by operator-splitting, Journal of Computational Physics 1986, 62 (1), 40-65. DOI: 10.1016/0021-9991(86)90099-9
22. F. R. Menter, Two-Equation Eddy-Viscosity Turbulence Models for Engineering Applications, AIAA Journal 1994, 32(8).
23. S. Pankatar, Numerical Heat Transfer and Fluid Flow, Taylor & Francis, 1980.
24. J.E. Rossiter, Wind-Tunnel Experiments on the Flow over Rectangular Cavities at Subsonic and Transonic Speeds, Aeronautical Research Council Reports and Memoranda, p. 3438, 1964.
25. R. Ma, P.E. Slaboch, S.C. Morris, Fluid mechanics of the flow-excited Helmholtz resonator, J. Fluid Mech. 2009, 623, 1-26. DOI: 10.1017/S0022112008003911
26. S. Weyna, Rozpływ energii akustycznych źródeł rzeczywistych (in Polish), WNT, 2005.